A Quantum Dynamics Study of $D_2 + OH \rightarrow DOH + D$ on the WSLFH Potential Energy Function†

Paolo Defazio

Dipartemento di Chimica, Universita' di Siena, Via A. Moro, 53100 Siena, Italy

Stephen K. Gray*

Chemistry Division, Argonne National Laboratory, Argonne, Illinois 60439

Received: February 11, 2003

The quantum dynamics of the reaction $D_2 + OH \rightarrow DOH + D$ on the Wu−Schatz−Lendvay−Fang−Harding ab initio-based potential energy function is investigated. A recently developed four-atom implementation of the real wave packet method is employed. Extensive six-dimensional calculations for a total angular momentum of $J = 0$ and, within the helicity-decoupled approximation, numerous $J > 0$ calculations are performed. Cross sections and rate constants for reaction are estimated using a *J*-shifting procedure and compared with quasi-classical trajectory, transition state theory, and experimental results. The results are also contrasted with comparable results for $H_2 + OH$. A surprising feature is that our rate constants agree best with zero-curvature transition state theory results, indicating that tunneling may not be as important as expected.

I. Introduction

The reaction

$$H_2 + OH \rightarrow H_2O + H \tag{1.1}$$

and its reverse reaction, as well as isotopic analogues such as the main subject of this paper,

$$D_2 + OH \rightarrow DOH + D \tag{1.2}$$

continue to be a focus of current interest, as a recent review by Smith and Crim[1] will attest.

The presence of several light atoms facilitates accurate theoretical work on these systems and makes them ideal test beds of electronic structure and dynamics theories. In particular, over the past 10 years, some of the most impressive and trend-setting quantum dynamics calculations on four-atom systems have been performed on these reactions,[2−9] establishing the viability of full-dimensional four-atom scattering dynamics. Work within just the past few years includes full-dimensional rate-constant calculations with angular momentum effects treated rigorously,[5] as well as more extensive quantum dynamics results that are based on novel and more accurate potential energy surfaces[6−9] than the older, widely used Walch−Dunning−Schatz−Elgersma (WDSE)[10, 11] surface.

The purpose of the present paper is to present quantum dynamics results for reaction 1.2, on the basis of the Wu−Schatz−Lendvay−Fang−Harding (WSLFH) potential function,[12] for which complementary quantum dynamics work on reaction 1.1 has recently been published.[13] Although based on high-level ab initio calculations,[12] the WSLFH surface is probably not as good as the best of the surfaces developed by Zhang, Collins, and co-workers.[6−9] However, the availability of extensive quasi-classical trajectory and transition state theory calculations on the WSLFH surface[12,14] makes the corresponding quantum calculations also a point of interest, from the standpoint of learning the adequacy of these more approximate approaches.

Section II below outlines our theoretical methods, section III presents our results, and section IV concludes.

II. Methods and Computational Details

As in Ref. 13, the wave packet is written as

$$\psi^{J,K,p}(R,r_1,r_2,\theta_1,\theta_1,\varphi,t) = \sum_{j_1,k_1,j_2} C^{J,K,p}_{j_1,k_1,j_2}(R,r_1,r_2,t)\, G^{J,K,p}_{j_1,k_1,j_2}(\theta_1,\theta_2,\varphi) \tag{2.1}$$

where *J* denotes the total angular momentum quantum number ($J = 0, 1, 2,...$), *K* is its projection on a body-fixed axis, and *p* is the parity ($p = +1$ or -1). The centrifugal sudden (CS) or helicity-decoupled approximation (i.e, the neglect of Coriolis coupling between different *K*-states[15,16]) is adopted, which has been shown to be a good approximation for the $H_2 + OH$ system.[5] Diatom−diatom Jacobi coordinates are employed: *R* is the distance between the D2 and OH centers of mass and the body-fixed axis is associated with *R*; r_1 is the D−D internuclear distance, and r_2 is the OH internuclear distance. The polar angles θ_1 and θ_2 are associated with the angles between the D_2 and OH bond vectors and *R*, and φ is the dihedral angle. $G^{J,K,p}_{j_1,k_1,j_2}(\theta_1,\theta_1,\varphi)$ is a parity-adapted rotational basis function[13] that also depends on the diatomic angular momentum quantum numbers for diatom 1, j_1,k_1, and diatom 2, j_2 (with k_2 being determined via $k_1 + k_2 = K$). With parity adaptation, it is possible to restrict the *K*-index to values $K \geq 0$. (Note that, for $K > 0$, k_1 can still be negative.) Neglecting Coriolis coupling, as we do here, and focusing on a particular j_1,j_2 initial state, the upper limit of *K* is $\min(J, j_1 + j_2)$. Each value of *K* (including $K = 0$) has $p = +1$ and -1 uncoupled parity states. For $K > 0$, the $+1$ and -1 parities yield the same Hamiltonian matrix

† Part of the special issue "Donald J. Kouri Festschrift".

* Author to whom correspondence should be addressed. E-mail: gray@anchim.chm.anl.gov.

10.1021/jp030190a CCC: $25.00
Published on Web 05/20/2003

elements (within the CS approximation) and, thus, generate the same dynamics; therefore, only calculations for one parity block with $K > 0$ need to be performed. For $K = 0$, the parity blocks are not equivalent and, depending on what is desired, a separate calculation for each parity may need to be performed.

The time evolution of a given initial wave packet is performed with the real wave packet method,[17] which is a more explicitly time-dependent interpretation of Mandelshtam and Taylor's damped Chebyshev iterations[18] and Kouri and co-workers time-independent wave packet ideas.[19] Flux techniques are used to infer the energy-resolved reaction probabilities from the real part of the evolving wave packet.[20] Further details of the particular four-atom Hamiltonian that we employ in this study may be found in Ref. 13.

The reactive cross section for reactants $D_2(v_1,j_1)$ and $OH(v_2,j_2)$ is

$$\sigma_{v_1 j_1, v_2 j_2}(\epsilon) = \frac{\pi}{2\mu\epsilon}\sum_J (2J+1) P^J_{v_1 j_1, v_2 j_2}(\epsilon) \qquad (2.2)$$

where $\mu = (2m_D)(m_H + m_O)/(2m_D + m_H + m_O)$, ϵ is the collision energy, and

$$P^J_{v_1 j_1, v_2 j_2}(\epsilon) = \frac{1}{(2J_1+1)(2J_2+1)}\sum_{K,p,k_1} P^{J,K,p}_{v_1 j_1, v_2 j_2}(\epsilon) \quad (2.3)$$

is the average reaction probability for a given total angular momentum J. The rate constant may be written as

$$k(T) = \frac{Q_{elec}(T)}{Q_r(T)} \sum_{v_1 j_1, v_2 j_2} g_{j_1 j_2} \exp[-\epsilon_{v_1 j_1, v_2 j_2}/(k_B T)]\, k_{v_1 j_1, v_2 j_2}(T) \qquad (2.4)$$

with

$$k_{v_1 j_1, v_2 j_2}(T) = \left(\frac{8k_B T}{\pi\mu}\right)^{1/2} \frac{1}{(kT)^2}\int_0^\infty d\epsilon\, \epsilon \exp[-\epsilon/(k_B T)]\sigma_{v_1 j_1, v_2 j_2}(\epsilon) \quad (2.5)$$

$Q_{elec}(T)$ accounts for the spin−orbit splitting of OH,[14] and $Q_r(T)$ is

$$Q_r(T) = \sum_{v_1 j_1, v_2 j_2} g_{j_1 j_2} \exp\left[-\frac{\epsilon_{v_1 j_1, v_2 j_2}}{k_B T}\right] \qquad (2.6)$$

The nuclear/rotational degeneracy factor in eqs 2.4 and 2.6 is g_{j_1,j_2}. D has nuclear spin 1; therefore, D_2 can have total nuclear spins 2, 1, and 0, with degeneracies 5, 3, and 1. Even j_1 levels occur with even total nuclear spins, and odd j_1 levels occur with odd nuclear spins. Therefore, $g_{j_1,j_2} = 6(2J_1 + 1)(2J_2 + 1)$ if j_1 is even, and $3(2J_1 + 1)(2J_2 + 1)$ if j_1 is odd. Actually, simply ignoring nuclear spin and using $(2J_1 + 1)(2J_2 + 1)$ as the degeneracy factor leads to rate constants that agree, to two significant figures, with those computed with the correct degeneracy factor for the moderate to high ($T \geq 250$ K) temperatures studied here.

Even for just a four-atom system, a complete quantum mechanical calculation of the rate constant, $k(T)$, is still a challenging computational problem, because of the large number of total angular momenta J (and associated states for given J) that must be considered. There are numerous strategies for calculating or approximating $k(T)$, many of which are based on cumulative reaction probability ($N(E)$) ideas.[21] $N(E)$ is the sum of all possible reactive transition probabilities, as a function of total system energy E, and the Boltzmann average of $N(E)$ is proportionate to $k(T)$. One extremely useful (approximate) approach is J-shifting.[22] The original J-shifting idea involves a full calculation of the $J = 0$ cumulative reaction probability as a function of energy, $N^{J=0}(E)$, and then assuming that the $J > 0$ contributions to $N(E)$ have the same functional form as the $J = 0$ result but are shifted in energy, relative to this result, to reflect centrifugal barriers at the transition state.

Here, we adopt a related approach to estimating cross sections and rate constants on the basis of the modified J-shifting procedure of Ref. 13. This procedure allows us to estimate certain state-resolved cross sections or rate constants and to later combine the results to estimate the fully averaged quantity, $k(T)$. Reference 13 showed, for the $H_2 + OH$ system, that this type of procedure led to a better estimate of the actual rate constant than the simplest J-shifting procedure outlined previously. For a specific initial reactant combination, v_1,j_1,v_2,j_2, and some appropriately "typical" J (J_{ref}), we evaluate eq 2.3 to obtain

$$p_{v_1 j_1, v_2 j_2}(\epsilon) \equiv P^{J_{ref}}_{v_1 j_1, v_2 j_2}(\epsilon) \qquad (2.7)$$

We then construct either state-resolved cross sections (eq 2.2) or rate constants (eq 2.5), via the J-shifting approximation:

$$P^J_{v_1 j_1, v_2 j_2}(\epsilon) \approx p_{v_1 j_1, v_2 j_2}[\epsilon' = \epsilon + (E^J_{ref} - E^J)] \qquad (2.8)$$

with E^J denoting the mean centrifugal barrier at the transition state,

$$E^J = \frac{1}{n_J}\sum_K (\bar{B}J(J+1) + (A - \bar{B})K^2) n_{JK} \qquad (2.9)$$

where n_{JK} is the number of possible initial conditions for given values of J and K, and n_J is the total number of initial conditions for given J. (For example, if $j_1 = j_2 = 2$, then the largest K can be is 4, and, for any $J \geq 4$, the sum of all the allowed k_1 and K combinations such that $k_1 + k_2 = K$ is $n_J = 25$ or the rotational degeneracy $(2J_1 + 1)(2J_2 + 1) = 25$.) If A, B, and C are the rotor constants at the transition state, which here is assumed to be an almost prolate symmetric top, $\bar{B} = (B + C)/2$. (For the D_2OH transition state, we find $A = 25.71$ cm^{-1}, $B = 1.47$ cm^{-1}, and $C = 1.39$ cm^{-1}.)

To estimate $k(T)$, we use a generalization of the approach in Ref. 13, which should be suitable for a wider temperature range. We choose a particular set of $\{v_1,j_1,v_2,j_2\}$ states and perform state-specific rate-constant calculations, as outlined previously with the modified J-shifting procedure. A reasonable estimate of the full rate constant is then provided by

$$k(T) \approx \frac{Q_{elec}(T)}{Q_{r\{v_1 j_1, v_2 j_1\}}(T)} \sum_{\{v_1 j_1, v_2 j_2\}} g_{j_1 j_2} \exp\left[-\frac{\epsilon_{v_1 j_1, v_2 j_2}}{k_B T}\right] k_{v_1 j_1, v_2 j_2}(T) \qquad (2.10)$$

where the brackets around the summation index terms ($\{...\}$) indicates that the sums are restricted to a particular set of reactant states. The set corresponding to $v_1 = v_2 = 0$ and all permutations of j_1 and j_2 with j_1, $j_2 \leq 4$ should yield reasonably accurate estimates of the rate constants for $T \leq 1000$ K. (At $T = 300$ K, $j_1 = 2$ and $j_2 = 2$ are the two most populous states, and at $T = 1000$ K, $j_1 = 2$ and $j_2 = 4$ are the two most populous states.) We explicitly performed all relevant propagations to obtain (for a given J_{ref}) reaction probabilities for $(j_1,j_2) = (0,0)$, (1,0), (1,1), (1,2), (2,0), (2,1), (2,2), (3,0), and (4,0). Because of the known

weak dependence of the reaction probabilities on the OH rotational quantum number, j_2, we can approximate the various missing j_1, j_2 probabilities by a calculated probability with the same j_1 value.

It is important to note that the general idea of including the effects of nonzero total angular momentum dynamics in *J*-shifting and related approximate rate-constant theories is not unique to this work or the work in Ref. 13. (See, for example, earlier work by Truhlar and co-workers,[23] Miller and co-workers,[24] Bowman and Shnider,[25] and Zhang and Zhang.[26]) It is difficult to comment reliably on the relative merits of all these approaches under the present circumstances without explicitly applying these methods to the present problem, and without knowledge of the exact quantum rate constant for the WSLFH surface.

The numerical Hamiltonian representation of Ref. 13 is employed: R and r_1 are described by evenly spaced grids, and the dispersion-fitted finite-difference approximation[27] is used for the action of the relevant kinetic-energy operator terms; r_2 is described with a two-point potential optimized discrete variable representation.[28,29] The propagation of a given initial state, characterized by quantum numbers J, K, v_1, j_1, v_2, j_2, k_1 and an incoming Gaussian wave packet in R, with appropriate energy spread, is analyzed to yield the relevant reaction probabilities over a range of energies, as in Ref. 13. To achieve convergence of the relevant reaction probabilities for collision energies $\epsilon \leq 1$ eV, experimentation has led to rotational basis sets with $j_1 = 0, 2, \ldots, 14$ or $1, 3, 5, \ldots, 15$ and $j_2 = 0, 1, \ldots, 9$. For example, with $K = 0$, $p = +1$, we have 345 (even j_1) or 370 (odd j_1) rotational basis states, whereas if $K = 1$, we have 605 (even j_1) and 655 (odd j_1) rotational basis states; i.e., the basis sets are approximately twice the size of those used previously[13] for H_2 + OH. The radial grid details were similar to those previously used[13] and ~4000 Chebyshev iterations were required for each propagation. We also employed the product analysis "trick" outlined in Ref. 30 to further refine our reaction probabilities. A typical propagation requires almost a full day of computational time on a 667 MHz, Compaq model XP1000 ("Dec-Alpha") workstation and up to 400 MB RAM. (Calculations were also performed on a Linux cluster of 1 GHz Pentium III computers with each calculation, despite the higher clock speed, now requiring up to 2 days of computation time. Of course, in this case, many simultaneous calculations can be performed.)

III. Results

A. Reaction Probabilities. Figure 1 displays various probabilities for reaction 1.2. Figure 1a shows solid probabilities for $J = 0, 10, \ldots, 50$ for reactants in their ground states. The dashed curve corresponds to our $J = 0$ result, and the solid curves are the predictions for $J = 10$, 20, 30, 40, and 50, based on *J*-shifting this $J = 0$ result (section II). The open circles correspond to the results of our actual CS (or helicity-decoupled) quantum dynamics calculations. We see that *J*-shifting is a reasonable estimator of the trends but tends to overestimate the reaction probabilities as J increases. For a collision energy of 0.6 eV, for example, the $J = 30$ reaction probability is overestimated by 20%.

In addition to reaction out of ground-state reactants, numerous excited reactant state combinations were investigated. Figure 1b displays some *J*-dependent reaction probabilities for $v_1 = 0$, $j_1 = 2$, $v_2 = 0$, $j_2 = 2$, averaged over all other angular momentum components (eq 2.3). (We focus on fewer J states than in Figure 1a because, as discussed in section II, $n_J = 25$ k_1,k_2 or k_1,p combinations must be considered for each $J \geq 4$. Allowing for the equivalence of even and odd parity Hamiltonians within the CS approximation for $K > 0$, the number of unique propagations required per J is 15, still requiring a large effort per J.) This particular reactant-state combination is one of the most important ones for room temperature. The dashed curve corresponds to the $J = 8$ quantum dynamics result, which was used as a basis for the modified *J*-shifting procedure outlined in section II (i.e., $J_{ref} = 8$). Solid curves correspond to shifts of this reaction probability and, as in Figure 1a, the open circles are the results of our quantum dynamics calculations. Because a large number of calculations are required for each $J > 0$ result, we have limited the comparison to just a few J cases. Nonetheless, it would appear that the modified *J*-shifting procedure for excited-state reactants is also quite reasonable.

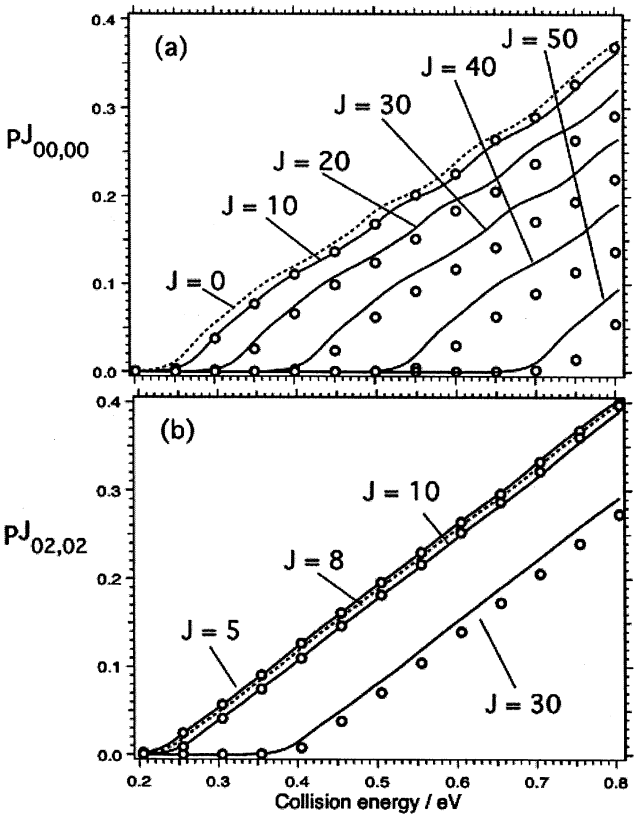

Figure 1. Centrifugal sudden (CS) total reaction probabilities for reaction 1.2 for reactants (a) $(v_1,j_1,v_2,j_2) = (0,0,0,0)$ and (b) $(v_1,j_1,v_2,j_2) = (0,2,0,2)$. In each panel, the dashed curve and symbols represent our calculated results and the solid curves represent predictions of the other J results based on $J_{ref} = 0$ in panel a and $J_{ref} = 8$ in panel b. See text for further discussion.

B. Cross Sections. The calculations summarized in Figure 1a allow one to estimate the initial ground-state ($v_1 = j_1 = v_2 = j_2 = 0$) state-specific cross sections. Figure 2 depicts some of the results that we have obtained. The CS result (lowest, dotted curve) is an explicit evaluation of eq 2.2, based on the CS reaction probabilities in Figure 1a and linear interpolation for J values for which we did not perform quantum calculations. This represents our best state-resolved cross section estimate for this case.

The other curves in Figure 2 correspond to the evaluation of eq 2.2 but with the modified *J*-shifting reaction probabilities based on $J_{ref} = 8$. Motivation for this choice of J_{ref} is provided by inspecting the relative contributions of the various J terms to the CS cross section. For collision energies near 0.3 eV, the $4 \leq J \leq 16$ range accounts for almost the entire cross section,

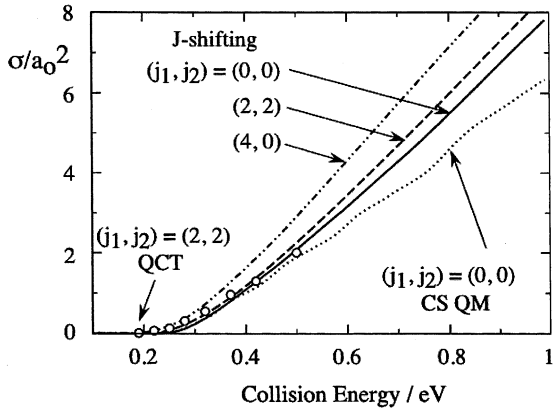

Figure 2. Initial state-resolved reactive cross sections for reaction 1.2. In all cases, $v_1 = v_2 = 0$ and the particular (j_1,j_2) initial state is indicated. Modified *J*-shifting based on $J_{ref} = 8$ was used to infer the (0,0), (2,2), and (4,0) cross sections, and the centrifugal sudden (CS) result for (0,0) is also displayed. Open circles represent the $(j_1,j_2) = (2,2)$ QCT results of Ref. 14, multiplied by 2 (because those results originally included a factor of 0.5 for the electronic degeneracy factor, which is not included in our results).

TABLE 1: $v_1 = j_1 = v_2 = j_2 = 0$ State Resolved Rate Constants for $D_2(v_1, j_1) + OH(v_2, j_2) \rightarrow HOD + D$

		$Q_{elec}k_{00,00}$ ($\times 10^{-16}$ cm^3 molecule^{-1} s^{-1})	
T (K)	Q_{elec}	CS	*J*-shifting
250	0.69	0.53	0.49
300	0.66	3.3	3.2
350	0.64	13.3	12.9
400	0.62	29.2	38.6

with $J = 8$ being the peak region. (For consistency, we therefore conducted an additional CS propagation with $J = 8$ and ground-state reactants to obtain the relevant reference reaction probability.) Comparison of the $(j_1,j_2) = (0,0)$ modified *J*-shifting (solid curve) and the more accurate CS results (dotted curve) in Figure 2 shows that we might expect good accuracy (10%) in the *J*-shifting approximation for collision energies of ≤ 0.5 eV and reasonable accuracy (20%) for collision energies up to 1 eV.

Troya et al.[14] conducted some quasi-classical trajectory (QCT) calculations for $D_2 + OH$ on the WSLFH potential surface. In particular, they determined the $v_1 = v_2 = 0$ and $(j_1,j_2) = (2,2)$ energy-resolved total cross section in the $\epsilon = 0.2-0.5$ eV range. Their results are displayed as open circles in Figure 2. (The explicit results presented in Fig. 6 of Ref. 14 include a factor of 0.5, the high-temperature limit of Q_{elec}, to account for the electronic degeneracy. We have therefore multiplied those results by 2 to compare with our results.) Our $(j_1,j_2) = (2,2)$ quantum results agree reasonably well with these QCT results. At $\epsilon = 0.5$ eV, the QCT cross section is $(2.0 \pm 0.1)a_0^2$, just 13% lower than our *J*-shifting result of $2.3a_0^2$. At lower ϵ, however, the QCT results tend to be larger than the quantum results. Still, at the relatively low ϵ value of 0.25 eV, the QCT cross-section result, $(0.13 \pm 0.02)a_0^2$ is in reasonable accord with our *J*-shifting result of $0.09a_0^2$.

C. Rate Constants. We determined both certain state-resolved rate constants and the full thermal rate constant, according to the procedures discussed in section II. The $k_{00,00}$ rate constant is useful because we can compare it to both the presumably more correct CS-based results and the modified *J*-shifting results. Table 1 compares these rate constants for moderate to low temperatures, showing that they agree remarkably well. Interestingly, the *J*-shifting result only becomes noticeably larger than the CS result (as would be expected on the basis of Figures 1 and 2) for $T \geq 400$ K.

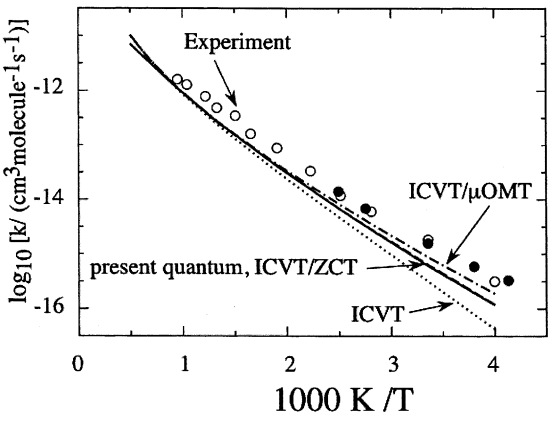

Figure 3. Arrhenius plot of the thermal rate constant for $D_2 + OH \rightarrow HOD + D$. Solid curve denotes our quantum estimate, unconnected open symbols are experimental results of Ref. 31, and filled symbols are data obtained from Ref. 32. The transition state theory results of Ref. 14 are also shown: $(\cdots)$ CVT, $(- - -)$ ICVT/ZCT (difficult to discern from our quantum results) and $(- \cdot - \cdot -)$ ICVT/μOMT.

TABLE 2: Various Thermal Rate Constant (k) Estimates at $T = 298$ K for $D_2 + OH \rightarrow HOD + D$

level	k ($\times 10^{-16}$ cm^3 molecule^{-1} s^{-1})
best quantum estimate, present calculations	6.3
$Q_{elec}k_{02,02}$, present calculations	6.2
ICVT[a]	3.15
ICVT/ZCT	6.38
ICVT/μOMT	8.73
experiment, 1981[b]	18.3 ± 1.2
experiment, 1996[c]	16.4 ± 1.3

[a] The transition state theory (ICVT) results are from Troya et al.[14] [b] Data from Ravishankara et al.[31] [c] Data from Talukdar et al.[32]

The full thermal rate constant for reaction 1.2 was also estimated using the procedures outlined in section II. Figure 3 displays the standard Arrhenius plot (solid curve) inferred from our calculations. Experimental results,[31,32] as well as the improved canonical variational transition state theory (ICVT)[33] results of Ref. 14, are shown. Our quantum estimate of the rate constant (solid curve) tends to be lower than the experimental results (unconnected solid symbols), particularly at lower temperatures. Table 2 further quantifies our result for $T = 298$ K. We see, for example, that the best quantum estimate of the rate constant is a factor of 2.6 smaller than the more recent experimental result.[32] This situation is quite similar to the underestimation of the $H_2 + OH$ rate constant by a factor of 2.6, found in previous calculations on the WSLFH surface.[13]

We should note that the (estimated) quantum rate-constant estimates of Ref. 9, based on the YZCL2 potential surface,[8] are in much better quantitative accord (20% or better) with the experimental data, implying that this potential surface may be superior to the WSLFH[12] surface employed here. Specifically, Zhang and co-workers[9] estimate a rate constant of 21.0×10^{-16} cm^3 molecule^{-1} s^{-1} at $T = 301$ K, which is in very good accord with the experimental result[32] at this temperature, $(18.0 \pm 0.7) \times 10^{-16}$ cm^3 molecule^{-1} s^{-1}.

Table 2 also shows that $Q_{elec}k_{02,02}$, which is the thermal rate-constant estimate that is based on just the most populous reactant state at 298 K, is quite close to the best result, which considered contributions from $j_1, j_2 \leq 4$. (Even by temperatures as high as 1000 K, we find that the difference between $Q_{elec}k_{02,02}$ and our best estimate is typically <10%.)

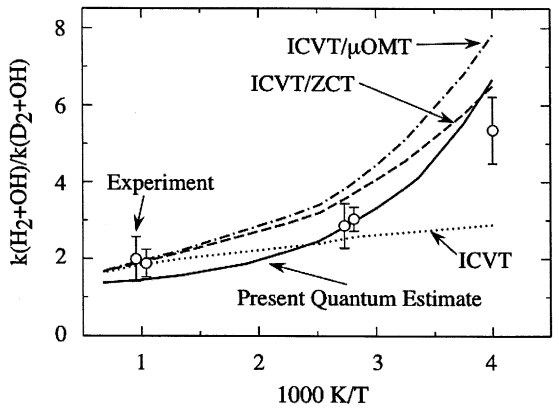

Figure 4. Our estimate of the ratio of the $H_2 + OH$ and $D_2 + OH$ rate constants. We also display experimental results,[31] and the various transition-state theory results of Ref. 14. Line styles are the same as those in Figure 3.

The comparison of our thermal rate constant results with the transition-state theory results is interesting. In Figure 3, the curve labeled ICVT represents a variational transition state theory level with no tunneling corrections. The curve labeled ICVT/ZCT involves a relatively simple tunneling correction that does not involve reaction path curvature ("zero curvature tunneling"). The ICVT/μOMT curve represents a higher level of tunneling correction that is the larger result of certain tunneling paths that incorporate reaction path curvature ("microcanonical, optimized, multidimensional tunneling").[33] For $T < 1000$ K, the ICVT/ZCT result (dashed curve), on the scale of the figure, can hardly be discerned from our quantum result (solid curve). On the other hand, the ICVT/μOMT result, while agreeing better with experimental results, is higher. Table 2 also quantifies these results for $T = 298$ K, showing that the ICVT/ZCT result is just 1.3% higher than our best result, whereas the ICVT/μOMT result is 38% higher.

The ratio of the thermal rate constants for $H_2 + OH$ and $D_2 + OH$ is also of interest.[14] Figure 4 presents an estimate of this ratio, employing our present $D_2 + OH$ results and the previous quantum estimates of Ref. 13 for $H_2 + OH$. Note that Ref. 13 only used the most populous $H_2 + OH$ reactant state ($v_1 = 0$, $j_1 = 1$, $v_2 = 0$, $j_1 = 2$) at $T = 300$ K. However, it is quite likely that an improved estimate of the $H_2 + OH$ rate constant, based on the inclusion of more reactant states, would not be too different, because that is what we found here for $D_2 + OH$. Our calculations (the solid curve in Figure 4) show that the $H_2 + OH$ reaction is faster than the $D_2 + OH$ reaction over a wide temperature range with the largest effect at lower temperatures (larger $1/T$) most likely being due to the greater importance of tunneling in the $H_2 + OH$ reaction. Experimental data (open circles with error bars), inferred from data in Ref. 31, are also displayed that are in reasonable accord with our results. The agreement is particularly good in the room temperature regime. We also give the results from the transition state theory calculations of Ref. 14. As with just the $D_2 + OH$ rate-constant results in Figure 3, we see that the best transition state theory result (assuming that our own quantum estimate is the most correct result for the WSLFH surface) is the ICVT/ZCT level.

IV. Concluding Remarks

We have performed a variety of quantum dynamics calculations on the $D_2 + OH \rightarrow HOD + D$ reaction and estimated cross sections and rate constants. Our results, based on the WSLFH potential energy surface,[12] were compared with available quasi-classical trajectory, transition state theory, and experimental results. Consistent with previous results for the $H_2 + OH$ reaction,[13] it appears that the thermal rate constants are underestimated on the WSLFH surface, and the surface of Yang and co-workers[8,9] provides a more quantitative description.

The availability of a variety of transition state theory results[14] on the WSLFH surface allowed us to gauge the adequacy of these more approximate but easier to apply theories. Interestingly, we found that a low-level tunneling correction (ICVT/ZCT) led to results that were in better accord with our best quantum estimates than a higher-level tunneling correction that allows for reaction path curvature effects (ICVT/μOMT). Does this mean that reaction path curvature effects are less important than those that would be expected for this system (and also $H_2 + OH$)? We have examined plots of our evolving wave packets, as well as Fourier transforms of our wave packets, on selected, tunneling regime energies. These plots show little evidence of "corner cutting", in relation to the reaction path. However, there are other explanations for the relatively poor performance of the higher-level transition state theory. For example, the calculations of Ref. 14 did not employ any corrections for vibrational anharmonicity, which could be important.[27,28]

Acknowledgment. We dedicate this paper to Donald J. Kouri, whose work continues to influence us all. We thank Diego Troya, G. C. Schatz, and A. D. Isaacson for helpful discussions. We are also indebted to Carlo Petrongolo for providing additional advice and encouragement. P.D. was supported by the Italian MIUR. S.K.G. was supported by the Office of Basic Energy Sciences, Division of Chemical Sciences, Geosciences and Biosciences, U. S. Department of Energy, under Contract No. W-31-109-ENG-38.

References and Notes

(1) Smith, I. W. M.; Crim, F. F. *Phys. Chem. Chem. Phys.* **2002**, *4*, 3543.
(2) Manthe, U.; Seideman, T.; Miller, W. H. *J. Chem. Phys.* **1993**, *99*, 10078.
(3) Zhang, D. H.; Zhang, J. Z. H. *J. Chem. Phys.* **1994**, *101*, 1146.
(4) Neuhauser, D. *J. Chem. Phys.* **1994**, *100*, 9272.
(5) Manthe, U.; Matzkies, F. *J. Chem. Phys.* **2000**, *113*, 5725.
(6) Zhang, D. H.; Collins, M. A.; Lee, S.-Y. *Science* **2000**, *290*, 961.
(7) Yang, M.; Zhang, D. H.; Collins, M. A.; Lee, S.-Y. *J. Chem. Phys.* **2001**, *115*, 174.
(8) Yang, M.; Zhang, D. H.; Collins, M. A.; Lee, S.-Y. *J. Chem. Phys.* **2001**, *114*, 4759.
(9) Zhang, D. H.; Collins, M. A.; Lee, S.-Y. *J. Chem. Phys.* **2002**, *116*, 2388.
(10) Walch, S. P.; Dunning, T. H. *J. Chem. Phys.* **1980**, *72*, 1303.
(11) Schatz, G. C.; Elgersma, H. *Chem. Phys. Lett.* **1980**, *21*, 73.
(12) Wu, G.; Schatz, G. C.; Lendvay, G.; Fang, D.-C.; Harding, L. B. *J. Chem. Phys.* **2000**, *113*, 3150.
(13) Goldfield, E. M.; Gray, S. K. *J. Chem. Phys.* **2002**, *117*, 1604.
(14) Troya, D.; Lakin, M. L.; Schatz, G. C.; Gonzalez, M. *J. Chem. Phys.* **2001**, *115*, 1828.
(15) Pack, R. T. *J. Chem. Phys.* **1974**, *60*, 633.
(16) McGuire, P.; Kouri, D. J. *J. Chem. Phys.* **1974**, *60*, 2488.
(17) Gray, S. K.; Balint-Kurti, G. G. *J. Chem. Phys.* **1998**, *108*, 950.
(18) Mandelshtam, V. A.; Taylor, H. S. *J. Chem. Phys.* **1995**, *102*, 7390.
(19) Huang, Y.; Iyengar, S. S.; Kouri, D. J.; Hoffman, D. K. *J. Chem. Phys.* **1996**, *105*, 927.
(20) Meijer, A. J. H. M.; Goldfield, E. M.; Gray, S. K.; Balint-Kurti, G. G. *Chem. Phys. Lett.* **1998**, *293*, 270.
(21) Miller, W. H. *J. Phys. Chem. A* **1998**, *102*, 793.
(22) Bowman, J. M. *J. Phys. Chem.* **1991**, *95*, 4960.
(23) Mielke, S. L.; Lynch, G. C.; Truhlar, D. G.; Schwenke, D. W. *Chem. Phys. Lett.* **1993**, *216*, 441.
(24) Wang, H.; Thompson, W. H.; Miller, W. H. *J. Phys. Chem. A* **1998**, *102*, 9372.
(25) Bowman, J. M.; Shnider, H. M. *J. Chem. Phys.* **1999**, *110*, 4428.
(26) Zhang, D. H.; Zhang, J. Z. H. *J. Chem. Phys.* **1999**, *110*, 7622.
(27) Gray, S. K.; Goldfield, E. M. *J. Chem. Phys.* **2001**, *115*, 8331.

(28) Echave, J.; Clary, D. C. *Chem. Phys. Lett*. **1992**, *190*, 225.
(29) Wei, H.; Carrington, T., Jr. *J. Chem. Phys*. **1992**, *97*, 3029.
(30) Gray, S. K.; Goldfield, E. M.; Schatz, G. C.; Balint-Kurti, G. G. *Phys. Chem. Chem. Phys*. **1999**, *1*, 1141.
(31) Ravishankara, A. R.; Nicovich, J. M.; Thompson, R. L.; Tully, F. P. *J. Phys. Chem.* **1981**, *85*, 2498.
(32) Talukdar, R. K.; Gierczak, T.; Goldfarb, L.; Rudich, Y.; Madhava Rao, B. S.; Ravishankara, A. R. *J. Phys. Chem.* **1996**, *100*, 3037.
(33) Truhlar, D. G.; Garrett, B. C.; Klippenstein, S. J. *J. Phys. Chem.* **1996**, *100*, 12771 and references therein.
(34) Isaacson, A. D.; Truhlar, D. G. *J. Chem. Phys.* **1982**, *76*, 1380.
(35) Isaacson, A. D. *J. Chem. Phys.* **1997**, *107*, 3832.